ARTICLE   **Open Access**

Enhancing the rectification effect of hydrogel-based stretchable ionic diodes through incorporating cations with high valence

Pengfei Xu[1], Xia Wu[1], Zefang Zhang[1], Peng Pan[1] and Xinyu Liu[1,2✉]

Abstract

The controlled migration of ions in biological systems has inspired the development of ion-based electronics. Ionic diodes, leveraging ions as charge carriers, offer selective control over ion flux, mimicking ion-selective behavior observed in biological systems. Conventional ionic diodes containing fluids encounter challenges in adapting to biological systems due to their limited stretchability and stability. Recent advancements in solid-state ionic diodes based on stretchable gels enable tissue-like stretchability while maintaining diode-like performance. However, their relatively low rectification ratio hinders their electrical performance, necessitating effective strategies to enhance the rectification effect of stretchable ionic diodes. Here, we propose a method to enhance the rectification effect of hydrogel-based stretchable ionic diodes by incorporating high-valence cations into the P-type hydrogel layer. Through neutralization reactions, cations with valences of 1, 2, and 3 were introduced to replace original hydrogen ions in the hydrogel, resulting in a substantial increase in the rectification ratio from 3 to over 70, with an elevated rectification ratio (140) under 100% strain. The enhanced rectification effect enables applications in iontronics, such as ionic rectifiers and bipolar junction transistors (BJTs). This study, for the first time, highlights the potential of improving electrical performances of iontronics through the manipulation of different ion properties.

Introduction

The spatiotemporally controlled migration of ions is widely involved in the biological domain[1–3]. It plays significant roles ranging from mediating communications between cells to the sensory perception in human skins[4,5]. To replicate such an ion-selective behavior and leverage it for normal bodily sensing and signal processing, the ionic diodes, in which ions serve as the charge carriers, have emerged as prominent iontronic devices enabling the regulation of ion migration and rectification of ionic currents[6–10]. Unlike conventional electronic diodes that rely on electrons, ionic diodes offer a more direct interface with biological systems as they share the same type of charge carriers; therefore are promising candidates for

the development of next-generation neuromorphic devices[11–14], ionic circuits[15,16] and human–machine interactions[17,18].

Early endeavors on ionic diodes employed charged membranes, nanochannels, or polyelectrolytes-modified carbon nanotubes to create micro-/nano-fluidic devices, selectively controlling the migrations of cations and anions through the channel via external voltage modulation[19–22]. However, the presence of liquid solutions and fluidic channels in these devices limited their adaptability to biological systems due to their low stretchability and high rigidity. More recently, solid-state ionic diodes based on gels have been designed to address the instability and low stretchability inherent in fluidic-based counterparts. By establishing a PN junction using two pieces of stretchable gels with oppositely charged polyelectrolytes, the ionic gel system behaves as a diode while maintaining a tissue-like stretchability (i.e., elongation at break >100%)[7]. For instance, ionic diodes constructed with double-network hydrogels exhibited a stretchability

Correspondence: Xinyu Liu (xyliu@mie.utoronto.ca)
[1]Department of Mechanical and Industrial Engineering, University of Toronto, Toronto, ON M5S 3G8, Canada
[2]Institute of Biomedical Engineering, University of Toronto, Toronto, ON M5S 3G9, Canada

exceeding 400% strain[23], and the solvent-free ionogel-based ionic diode can be stretched up to 100%[14], showcasing superior mechanical compatibility with biological systems compared to rigid fluidic-based ionic diodes. Owing to their tissue-like stretchability and softness, gel-based ionic diodes hold significant potential as iontronics for skin-like sensors, energy harvesters, and soft semiconducting devices[24,25].

Despite achieving tissue-like ion-selective behavior and mechanical properties, stretchable gel-based ionic diodes still exhibit a relatively low rectification ratio. For instance, current hydrogel-based stretchable ionic diodes have a rectification ratio ranging from 2 to 50[7,23,26−28]. The solvent-free ionogel-based ionic diode showed an enhanced rectification ratio of 50 attributed to non-faradaic processes. The relatively low rectification ratio may limit the rectification effect of the ionic diode, thereby potentially impacting the electrical performance of the integrated iontronics. Efforts have been directed towards enhancing the rectification ratio of the ionic diode. Strategies include reducing the thickness of the positive–negative (PN) junction, utilizing microporous or reactive electrodes[14], and incorporating nanochannels or films into the device[22,29,30]. While these improvements have shown promising results in enhancing the electrical performance of ionic diodes, they often involve complex fabrication processes or structural design alterations that may compromise the device's stretchability. Therefore, material-level adjustments to enhance the diode's rectification effect would be preferable for improving adaptability and versatility across various applications.

Here, we utilized hydrogel-based stretchable ionic diodes as our platform and found a method to enhance their rectification effect by incorporating cations with high valence into the positive-type (P-type) hydrogel layer. High-valence cations were incorporated through neutralization reactions between mobile hydrogen ions (H^+) in the P-type hydrogel and added bases. We selected cations with the valence of 1, 2, and 3 to replace the pristine H^+ within the P-type hydrogel layer. With the replaced cations in the P-type layer, we studied the rectification effect of ionic diodes and observed that the rectification ratio would increase with the valence of cations. This adjustment resulted in a substantial increase in the rectification ratio, elevating it from 3 (with cations of valence 1) to over 70. Furthermore, the rectification ratio showed further enhancement under stretching, reaching a ratio exceeding 100 at 100% strain. Both the rectification ratio and stretchability surpassed those of most previously reported stretchable ionic diodes. The enhanced rectification effect allows us to apply the ionic diodes in iontronics such as ionic circuits. We demonstrated the functionality of our hydrogel-based ionic diodes by constructing ionic rectifiers and bipolar
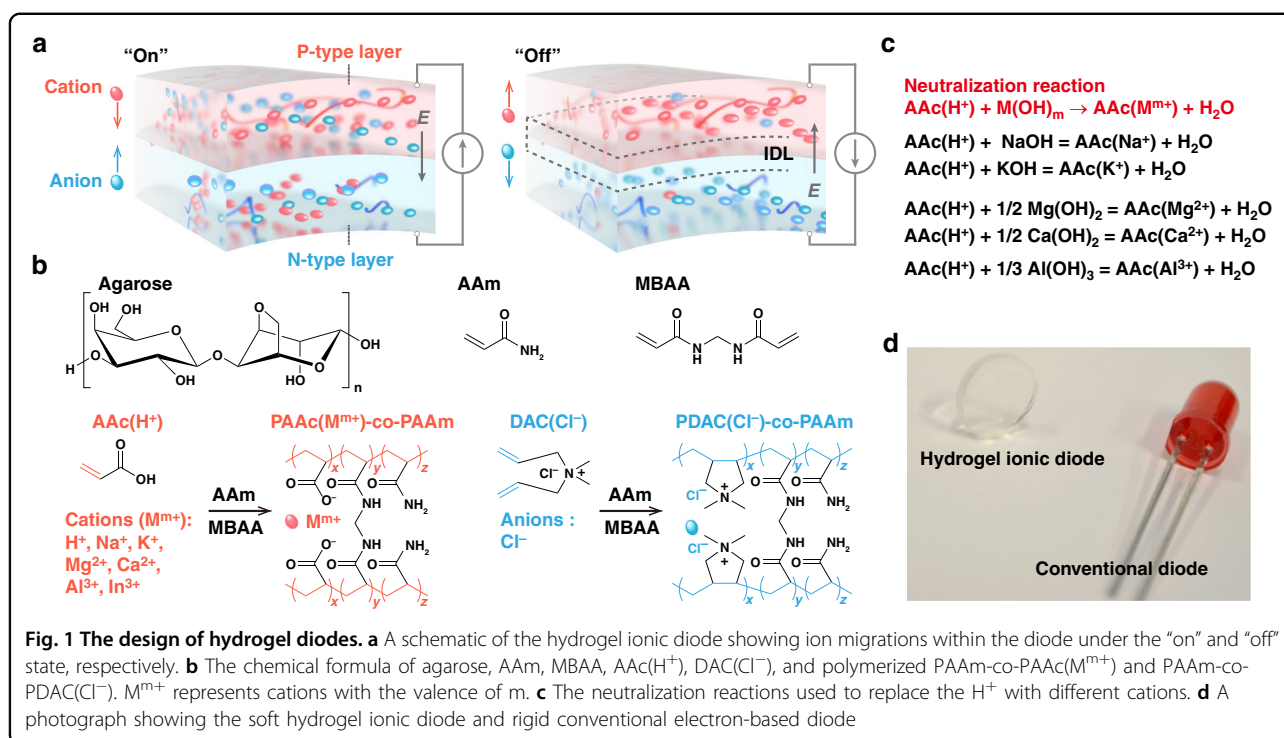
junction transistors (BJT), highlighting the promising applications of our approach in augmenting the performance of iontronics.

Results
Design of hydrogel diodes

Figure 1a shows a schematic of the hydrogel-based stretchable ionic diode, consisting of bilayer hydrogels with positively charged and negatively charged polyelectrolytes[23]. The P-type layer comprises negatively charged polyelectrolytes with mobile cations, while the N-type layer consists of positively charged polyelectrolytes with mobile anions. While the charged polyelectrolytes are normally immobilized in the P-type and negative-type (N-type) layers, the mobile cations and anions can be driven by the electric field applied to the hydrogel diode. When a forward electric bias is applied to the hydrogel diode as shown in the left schematic of Fig. 1a, the mobile cations in the P-type layer migrate towards the N-type layer, and vice versa, mobile anions in the N-type layer move towards the P-type layer, resulting in the ion accumulation. This movement of ions enhances the conductivity of the hydrogel and features an "on" state for the hydrogel diode. Conversely, when a reverse electric bias is applied, most mobile cations and anions in the P-type and N-type layer cannot traverse the bilayer interface. Instead, they form an internal electric field generated by the ionic double layer (IDL) at the PN interface, establishing a depletion region[14]. The presence of the depletion region limits current flow, leading to an "off" state for the hydrogel diode. As a result, the hydrogel bilayers function as a diode. The development of a gel-based ionic diode circumvents the need for leachable liquids and non-stretchable materials that were commonly used in the fluidic-based ionic diodes. In the meantime, the ion selectivity is achieved through the incorporation of oppositely-charged polyelectrolytes trapped in the gel matrix, eliminating the necessity for membranes[31] or nanochannels[32] and thus simplifying the device fabrication. All of these advantages are realized through the use of hydrogel networks that offer good stretchability and capability of immobilizing polyelectrolytes in a solid-state system[33,34]. Therefore, we employed the stretchable hydrogels to construct the ionic diode and evaluated its rectification effect and mechanical behaviors.

Here, we selected the double-network hydrogel as our material matrix for constructing the hydrogel diode due to its commonly acknowledged enhanced toughness and stretchability compared to single-network hydrogels[33,34]. Specifically, we employed the conventional agarose-polyacrylamide (Agar-PAAm)-based double-network hydrogel as the uncharged neutral polymer networks owing to its well-established mechanical properties and biocompatibility[35] (Fig. 1b). Within this system, the Agar

Fig. 1 The design of hydrogel diodes. a A schematic of the hydrogel ionic diode showing ion migrations within the diode under the "on" and "off" state, respectively. **b** The chemical formula of agarose, AAm, MBAA, AAc(H$^+$), DAC(Cl$^-$), and polymerized PAAm-co-PAAc(M^{m+}) and PAAm-co-PDAC(Cl$^-$). M^{m+} represents cations with the valence of m. **c** The neutralization reactions used to replace the H$^+$ with different cations. **d** A photograph showing the soft hydrogel ionic diode and rigid conventional electron-based diode

serves as a rigid polymer network to improve the toughness and the PAAm serves as a soft polymer network to enhance the stretchability. In our previous work[23], the polyelectrolytes were introduced into the double-network hydrogels by doping either positively charged polyelectrolytes such as poly(diallyldimethylammonium chloride) [PDAC(Cl$^-$)] or negatively charged polyelectrolytes such as sodium polystyrene sulfonate [PSS(Na$^+$)] into the Agar-PAAm hydrogel networks. However, the non-crosslinked polyelectrolytes had the potential to migrate under the applied electric field, potentially impacting the rectification ratio. Hence, in this work, instead of directly doping the PSS and PDAC polymers, we used a co-polymer system that is crosslinked by the neutral polymer PAAm and polyelectrolytes (Fig. 1b), aiming to mitigate the possible migration of isolate polyelectrolytes. For instance, for the P-type layer, the monomer acrylamide (AAm) was co-polymerized with monomer acrylic acid [AAc(H$^+$)] to produce negatively charged polyelectrolytes PAAc(H$^+$)-co-PAAm. As for the N-type layer, the AAm was copolymerized with [2-(Acryloyloxy)ethyl]trimethylammonium chloride [DAC(Cl$^-$)] to generate positively charged polyelectrolytes PDAC(Cl$^-$)-co-PAAm[23,36]. With the presence of crosslinker N,N'-methylenebisacrylamide (MBAA), the copolymers were crosslinked into a network (Fig. 1b). As a result, the crosslinked copolymers served as polyelectrolytes within the Agar-copolymer double-network hydrogels, where the mobile cations and anions acted as primary charge carriers that can be freely driven by the electric field.

As the primary mobile charge carriers within the hydrogel ionic diode, the properties of ions could possibly influence the overall electrical performance of the diode. Factors such as the ion size, mass, and charge may impact the rectification effect of the hydrogel diode. Here, we hypothesize that altering the valence of mobile ions within the hydrogel diode could potentially modulate the diode's ionic conductivity and modify its rectification ratio. To test this hypothesis, we incorporated cations with varying valences into the P-type hydrogel layer through neutralization reactions. This process allowed us to replace the original hydrogen ions (H$^+$) in AAc(H$^+$) (Fig. 1c). For instance, the sodium ions (Na$^+$) were introduced by adding the corresponding base sodium hydroxide (NaOH) into the acid monomer AAc(H$^+$). The molar ratio of NaOH and AAc(H$^+$) was set as 1:1 so the hydrogen ions in AAc(H$^+$) can fully react with hydroxide ions (OH$^-$) and form water. The Na$^+$ ions remained as mobile cations with the valence of 1. Thus, the pristine monomer AAc(H$^+$) was replaced to AAc(Na$^+$). This newly formed monomer AAc(Na$^+$) was further copolymerized with AAm and MBAA, and crosslinked into the polyelectrolytes network PAAc(Na$^+$)-co-PAAm (Fig. 1b). Various bases including sodium hydroxide (NaOH), potassium hydroxide (KOH), magnesium hydroxide [Mg(OH)$_2$], calcium hydroxide [Ca(OH)$_2$], and aluminum hydroxide [Al(OH)$_3$] were used to introduce Na$^+$, K$^+$, Mg^{2+}, Ca^{2+}, and Al^{3+}, respectively, into the P-type hydrogel layer. It should be noted that the In^{3+} were introduced by adding the salt indium(III) chloride (InCl$_3$) due to the poor

solubility of indium hydroxide [$In(OH)_3$]. To ensure complete reaction between H^+ and OH^-, the molar ratio of $AAc(H^+)$ to the added base [e.g., $M(OH)_m$ with the cation M^{m+} having a valence of m] was initially set as m:1 (Fig. 1c). For example, when incorporating cations with the valence of 2, such as Ca^{2+} and Mg^{2+}, the molar ratio of $AAc(H^+)$ and base [e.g., $Ca(OH)_2$ or $Mg(OH)_2$] was set as 2:1. It should be noted that for the N-type hydrogels, we used a copolymerized network $PAAm-co-PDAC(Cl^-)$ and did not replace the anions, due to the challenge of applying the same neutralization reaction to replace Cl^- ions. As a result, in our modified hydrogel diode, we can vary the valence of mobile cations in the P-type hydrogel, and the valence of mobile anions (Cl^-) in the P-type hydrogel remained as 1. By employing the crosslinked $PAAm-co-PAAc(M^{m+})$ P-type layer and $PAAm-co-PDAC(Cl^-)$ N-type layer, we could easily assemble a soft and stretchable hydrogel ionic diode by attaching the two layers together (Fig. 1d). With different mobile cations within the hydrogel diodes, we can assess the impact of mobile cations on the overall electrical performance.

We prepared the $PAAm-co-PDAC(Cl^-)$ N-type hydrogel layer and $PAAm-co-PAAc(M^{m+})$ P-type hydrogel layer with different cations. During the preparation of the P-type hydrogel layer, we observed that NaOH and KOH readily dissolved in water and efficiently reacted with $AAc(H^+)$. While $Mg(OH)_2$ and $Ca(OH)_2$ have lower solubility in pure deionized (DI) water, they can be fully dissolved with the presence of acid $AAc(H^+)$ and yield a colorless transparent hydrogel precursor. However, $Al(OH)_3$ is insoluble in water and cannot fully dissolve even with the presence of $AAc(H^+)$. As a result, at the molar ratio [$AAc(H^+):Al(OH)_3$] of 1:(1/3), the hydrogel precursor and cured hydrogels appeared white and opaque, due to undissolved $Al(OH)_3$ particles within hydrogels. To address this issue, we reduced the amount of $Al(OH)_3$ and adjusted the ratio of $AAc(H^+):Al(OH)_3$ to 1:(1/6), 1:(1/9), 1:(1/12), and 1:(1/15). One can see that the transparency of hydrogels increases with the decrease of $Al(OH)_3$ amount, indicating fewer undissolved $Al(OH)_3$ particles within hydrogels (Fig. S1). Similarly, indium(III) hydroxide [$In(OH)_3$] and zirconium(IV) hydroxide [$Zr(OH)_4$] have poor solubility in the $AAc(H^+)$ hydrogel precursor solution. Therefore, the maximum valence we chose was 3 due to the difficulty of neutralization reactions for bases containing high-valence cations. Following the preparation of the P-type and N-type hydrogels, we assembled the ionic diode by physically attaching the P-type and N-type layers together. When the P-type and N-type hydrogels are attached, the depletion of mobile cations and anions at the interface leads to the formation of electrostatic adhesion[23,27]. Shear tests confirm that the interfacial bonding strength between the P-type/N-type hydrogel layers is significantly higher than that of P-type/ P-type and N-type/N-type hydrogel layers (Fig. S2), validating the electrostatic adhesion driven by oppositely charged polyelectrolytes. The resulting diode was then cut into a circular shape with an overall thickness of 2 mm and a diameter of 8 mm for further electrical characterizations.

Enhanced rectification effect by incorporating high-valence cations

We first compared the electrical performance of hydrogel ionic diodes with different cations, by applying forward electric field and backward electric field to the diodes. Figures 2a and S3 show the current response of the hydrogel diode after a fixed time ($t_0 = 80$ s) of ion migrations until the current reached a plateau. The forward voltage bias and the backward voltage bias applied on the hydrogel diode were 5 and -5 V, respectively. One can see that for P-type layer with H^+, the current under the forward bias (I_f) is higher than that under the backward current (I_b), yielding an average rectification ratio (I_f/I_b) of 3.57, consistent with previously reported results[7,23,26–28]. Substituting the H^+-based P-type layer with the Ca^{2+} or Mg^{2+}-based P-type layer resulted in increased forward current and decreased backward current, indicating a higher rectification ratio. This trend was further validated if using Al^{3+} or In^{3+}-based P-type layer. Although their forward currents remained at a similar level (~2.75 mA) to those measured using the Ca^{2+} or Mg^{2+}-based P-type layer, their backward currents were notably lower (~0.06 mA for Al^{3+} and In^{3+}) compared to that using Ca^{2+} (~0.28 mA), Mg^{2+} (~0.48 mA), and H^+ (~0.55 mA). The lower backward current associated with high-valence cations suggests a superior ability to block the reverse current and an enhanced rectification effect. It should be noted that for K^+ and Na^+, they showed relatively high backward currents, indicating poorer rectification effects. This is possibly due to a high level of ion diffusions through the PN interface. The current–voltage (I–V) curves obtained by sweeping the applied voltage from 5 to -5 V further validated the enhanced rectification effect by using cations with high valence (Fig. S4). With the enhanced rectification ratio by introducing high-valence cations (e.g., Al^{3+} cations), an asymmetric I–V curve with a distinct reverse cut-off region can be obtained (Fig. S4). We summarized the rectification ratio and backward current of hydrogel diodes using H^+, K^+, Na^+, Mg^{2+}, Ca^{2+}, Al^{3+}, and In^{3+}, respectively (Fig. 2b). By increasing the valence of cations, the rectification ratio from diodes with trivalent cations was the highest, while the rectification ratio from diodes using monovalent cations was the lowest. The rectification ratio of using Mg^{2+} and Ca^{2+} ranged from 8 to 25, and the rectification ratio of using Al^{3+} and In^{3+} ranged from 42 to 77. On the other hand, backward current from diodes with
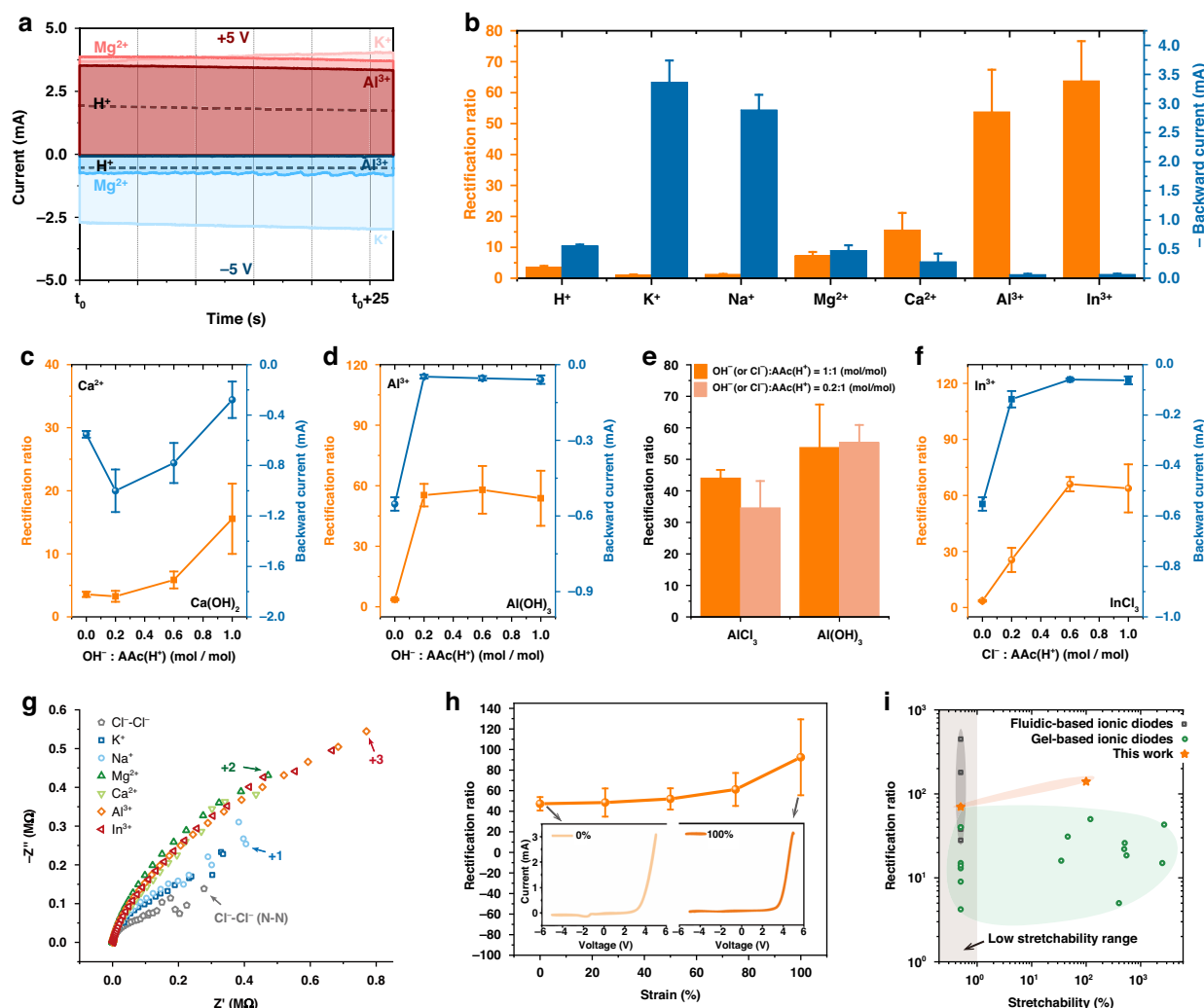
Fig. 2 Characterizations of hydrogel diodes. a The current response of hydrogel diodes with H^+, K^+, Mg^{2+}, or Al^{3+} after a fixed time ($t_0 = 80$ s) of ion migrations until the current reached a plateau, showing the decreased values of backward currents and enhanced rectification performances of diodes with high-valence cations. **b** The rectification ratios and backward currents of hydrogel ionic diodes with different cations including H^+, Na^+, K^+, Mg^{2+}, Ca^{2+}, Al^{3+}, and In^{3+}, showing the enhanced rectification ratios and decreased backward currents for diodes high-valence cations. **c** The rectification ratios and backward currents of hydrogel ionic diodes with different amounts of added $Ca(OH)_2$ and **d** $Al(OH)_3$. The Ca^{2+} and Al^{3+} were incorporated through $Ca(OH)_2$ and $Al(OH)_3$. **e** The rectification ratios of hydrogel diodes made with $AlCl_3$ and $Al(OH)_3$, respectively. **f** The rectification ratios and backward currents of hydrogel ionic diodes with different amounts of added $InCl_3$. The In^{3+} was incorporated through $InCl_3$. **g** The Nyquist plot of hydrogel ionic diodes with different cations, measured under a negative voltage bias of -5 V and sweeping frequency from 10^6 to 10^{-1} Hz, showing increased impedances of diodes with cations having higher valence. Here, $Cl^-–Cl^-$ represents a control sample made by two attached N-type hydrogel layers. **h** The rectification ratio of hydrogel ionic diodes with Al^{3+} under different stretching strains. The two insets show the rectification performance of diodes under the strain of 0% and 100%, respectively. **i** The Ashby plot of previously reported ionic diodes and our hydrogel ionic diodes comparing their rectification ratio and stretchability. Data points are from references labeled in Fig. S10 and Table S3

monovalent cations was substantially higher than that from diodes with trivalent cations. Overall, the rectification ratio was found to increase with the valence of cations, and the backward current decreased accordingly (Fig. 2b).

Then, we investigated how varying the amount of added bases would affect the rectification effect of the hydrogel diode. The amount of added bases is relevant to the extent of neutralization reactions. When the molar ratio of OH^-

in the bases and H^+ in the acid $AAc(H^+)$ equals 1:1, complete neutralization between the acid and base is anticipated. However, if a lesser amount of bases is added, it's possible that H^+ may not be entirely neutralized, resulting in excess monovalent cations (H^+) within the hydrogel system. We adjusted the molar ratio of OH^- (from the added bases) and $AAc(H^+)$ to be 0:1, 0.2:1, 0.6:1, and 1:1. It can be seen that for hydrogel diode with Ca^{2+} or Mg^{2+}, the rectification ratio increased with the

addition of bases and the backward current decreased accordingly (Figs. 2c and S5). The initial increase in backward current at a molar ratio [OH$^-$:AAc(H$^+$)] of 0.2 may be attributed to the coexistence of Ca^{2+} and H$^+$ in a mixed-cation system, which likely alters ion transport dynamics and enhances diffusion flux[37,38]. However, as the base concentration increases, the backward current steadily decreases, indicating an enhanced rectification effect once monovalent cations are mostly replaced by divalent cations. The highest rectification ratio was achieved at the molar ratio of 1:1. The results indicate that replacing more H$^+$ with high-valence cations can enhance the rectification effect. At the ratio of 0:1, 0.2:1, and 0.6:1, there was less OH$^-$ compared to H$^+$, resulting in incomplete replacement of H$^+$ with Ca^{2+} or Mg^{2+}. As a result, the extra H$^+$ in the hydrogel system affected the rectification effect. For hydrogel diode with Al^{3+}, the rectification ratio increased as the molar ratio of OH$^-$:AAc(H$^+$) changed from 0:1 to 0.2:1, but there was no substantial enhancement in the rectification effect as the molar ratio continued to increase to 0.6:1 and 1:1 (Fig. 2d). This can be attributed to undissolved Al(OH)$_3$ which failed to provide mobile Al^{3+}. This result aligns with our observations in Fig. S1, where Al(OH)$_3$ or In(OH)$_3$ cannot be fully dissolved in the AAc(H$^+$) solution. When the ratio of Al(OH)$_3$:AAc(H$^+$) was set to (1/15):1 [equivalent to a ratio of 0.2:1 for OH$^-$: AAc(H$^+$)], the hydrogel sample became fully transparent, indicating that the Al^{3+} were properly dissolved.

Due to the poor solubility of bases containing trivalent cations, we attempted to introduce trivalent cations into the hydrogel system using soluble salts such as aluminum chloride (AlCl$_3$) and indium(III) chloride (InCl$_3$). However, it should be noted that using salts like AlCl$_3$ or InCl$_3$ would introduce additional anions Cl$^-$ into the P-type layer. These extra anions in the P-type layer can migrate and induce reverse leakage current when the diode is under the backward electric field (in the "off" state), thereby negatively impacting the rectification effect. We prepared the hydrogel diode containing AlCl$_3$ and Al(OH)$_3$, respectively, and compared their rectification ratios and backward currents. For the hydrogel diode made from AlCl$_3$, the molar ratio of Cl$^-$:AAc(H$^+$) was 0.2:1. Similarly, for the hydrogel diode made from Al(OH)$_3$, the molar ratio OH$^-$:AAc(H$^+$) was set to 0.2:1. It can be seen that the hydrogel diode made from Al(OH)$_3$ showed a higher rectification ratio (average: 55.31) than that (average: 34.62) made from AlCl$_3$ (Fig. 2e). The backward currents of diodes made from Al(OH)$_3$ were lower than that made from AlCl$_3$ (Fig. S6). The lower rectification ratio and higher backward currents from diodes using AlCl$_3$ could be attributed to the extra anions Cl$^-$ that affected the rectification effect. As previously discussed, for hydrogel diode made from Al(OH)$_3$,

increasing the molar ratio of OH$^-$:AAc(H$^+$) from 0.2:1 to 1:1 did not significantly enhance the rectification effect due to the undissolved Al(OH)$_3$. While for hydrogel diode made from AlCl$_3$, increasing the molar ratio of Cl$^-$:AAc(H$^+$) from 0.2:1 to 1:1 could increase the amount of mobile Al^{3+} in the hydrogel system due to good solubility of AlCl$_3$. This increase also introduced extra Cl$^-$ into the P-type hydrogel, resulting in a lower rectification ratio and higher backward currents compared to that from the diode using Al(OH)$_3$. Similarly, we used InCl$_3$ to introduce In^{3+} into the hydrogel diode due to the poor solubility of In(OH)$_3$. It can be seen that the rectification ratio increased with the added amount of InCl$_3$ until the molar ratio of Cl$^-$:OH$^-$ reached 0.6:1 (Fig. 2f). However, further addition of InCl$_3$ did not lead to a significant increase in the rectification ratio, possibly due to the detrimental effect of the additional chloride ions Cl$^-$ on the rectification effects. We also characterized the effect of thickness to the diode rectification performance. As shown in Fig. S7, the rectification ratio of the hydrogel diode (cations: Al^{3+}) increases with the decrease of thickness. This can be attributed to the shorter ion migration distance and enhanced ion transport efficiency due to the thinner PN junction, therefore strengthening the rectification effect[37,39]. However, current fabrication constraints may limit the minimum achievable thickness. Although thin-film fabrication methods such as spin coating or spray coating can enable thinner hydrogel layers, the high water content and the increased surface-area-to-volume ratio of the hydrogel thin film could accelerate water evaporation, presenting a fabrication challenge that needs to be carefully addressed. To address this issue in the future, a more stable ionic diode system, such as an organogel or ionogel-based diode, could mitigate dehydration issues and potentially enable further thickness reduction for improved rectification performance.

In addition, we compared the frequency response of the hydrogel ionic diodes with different cations. Here, hydrogel diodes with Ca^{2+} and Al^{3+} were selected for this comparison due to their improved rectification effect. We applied triangle waves with the amplitude of 5 V and frequencies ranging from 0.01 to 2 Hz as the input, and measured the current response of the hydrogel diodes. It can be seen that for hydrogel diode with divalent cations Ca^{2+}, the reverse leakage current started to increase at the frequency of 0.05 Hz (Fig. S8). This can be attributed to the limitation of ion itself that cannot display a fast response to the high frequency input. The migration of ions requires sufficient time, and higher input frequencies result in shorter response time for ion migrations, thus affecting the rectification effect of diodes. However, although the reverse leakage current showed a similar trend of increase with the frequency, the hydrogel diode with trivalent cations Al^{3+} can maintain a

certain level of rectification effect even at the frequency of 1 Hz (rectification ratio: ~3). This observation suggests that incorporating cations with high valence can enhance the rectification effect in terms of the range of working frequencies.

Analysis of the enhanced rectification effect

Under the forward electric field, the mobile cations are driven by the electric field and migrate from the P-type layer to the N-type layer. Similarly, the mobile anions will migrate from the N-type layer to the P-type layer. The migrations of cations and anions accumulate at the PN interface, and form the forward current flow. On the contrary, under the backward electric field, the mobile cations and anions are driven to migrate towards the electrodes, impeding the ion flow through the PN interface, thereby establishing a reverse cut-off for the ionic diode. However, from our results in Fig. 2a, f, a non-negligible current flow (backward current) through the PN interface was observed when the backward electric field was applied. This non-negligible backward current indicated a certain level of ion flow through the PN interface, potentially impacting the rectification effect of the ionic diodes. We attribute this backward current to the ion diffusion through the PN interface. For instance, even under the backward electric field, the mobile cations in the P-type layer can still diffuse through the interface, and on the other hand, the anions in the N-type layer can diffuse from the N-type layer to the P-type layer, contributing to the backward current flow. Different cations with varying valences showed distinct levels of backward current. Therefore, their differing rectification ratios could be linked to the discrepancy in ion diffusion of cations. Here, we used electrochemical impedance spectroscopy (EIS) to investigate the impedance response of the reverse-biased diodes with different cations. By applying a backward voltage of −5 V to the ionic diodes, we recorded the impedance (including the real impedance Z' and imaginary impedance Z") while sweeping the frequency from 10^6 to 10^{-1} Hz (Figs. 2g and S9a). One can see that in the low frequency range, the impedance of diodes with high-valence cations was higher than that with low-valence cations, indicating that higher valence can lead to higher impedance for the diodes. This result aligns with our previous results in Fig. 2a, b, wherein the lower backward current observed in diodes with high-valence cations was attributed to their higher impedance.

We speculate that the higher impedance of diodes with high-valence cations (under the backward electric field) could be attributed to the fewer diffusions of ions. To further investigate this, we characterized the diffusion of cations in the ionic diodes. Given the linear correlation between the differential capacitance (C_{Diff}) and diffusion coefficients of ions[40,41], the ion-diffusion-based

mechanism could be further elucidated by comparing the capacitance derived from EIS. Utilizing the equation provided in the supplementary information [Eqs. ((1) and (2)) in the supplementary information] to determine the total impedance[42], we calculated the capacitance of the ionic diodes by measuring the slope of the impedance spectrum at the low-frequency region[43] (Fig. S9b). The calculated capacitance of diodes with different cations were summarized in Table S1. It can be seen that $C(M^{3+}$, e.g., Al^{3+}, $In^{3+}) < C(M^{2+}$, e.g., Mg^{2+}, $Ca^{2+}) < C(M^+$, e.g., Na^+, $K^+) < C(Cl^- - Cl^-)$. where "$Cl^- - Cl^-$" denotes the control sample, comprised of two pieces of N-type PDAC(Cl⁻)-co-PAAm hydrogel layers, which exhibited no rectification effects. The lower capacitance of diodes with high-valence cations (Al^{3+} and In^{3+}) suggests reduced diffusions within the ionic diodes. The diffusion coefficients of ions can be evaluated based on the Nernst–Einstein equation[44,45]:

$$D_{ion} = \frac{RT\Lambda^0}{|Z_{ion}|F^2}$$

where D_{ion} is the diffusion coefficient of the ion (m²/s), Λ^0 is the molar conductivity, R is the gas constant, T is the temperature, F is the Faraday constant, and Z_{ion} is the charge number of the ion. The ion diffusion coefficients are related to the charge number of ions and the molar conductivity of the ion. The molar conductivity of the ion is related to the number of moles of cations. In our work, to maintain consistent charge concentration of cations within the diode, we kept the number of moles [i.e., ν (mol)] of added cations proportional to the valence, such that $\nu(M^{3+}) = (1/3)\nu[AAc(H^+)]$, $\nu(M^{2+}) = (1/2)\nu[AAc(H^+)]$, $\nu(M^+) = \nu[AAc(H^+)]$. This approach indicated that the concentration of cations decreased with the increasing valence (see Table S2 and details in the supplementary information). Hence, the conductivity of cations (Λ^0) in the diodes can be written as Eqs. (14)–(16) in the supplementary information, wherein the conductivity of ions is related to the valence (Z_{ion}) and ionic conductivity (Λ_+) of the cation. Therefore, for systems with the same charge concentrations, higher valence leads to a lower the diffusion coefficient (see details in the supplementary information). In addition, we checked literature and summarized the diffusion coefficients and molar conductivity of different cations in Table S2. It should be noted that the diffusion coefficients were calculated based on equivalent charge concentrations (e.g., $1/3M^{3+}$, $1/2M^{2+}$, and M^+ sharing identical charge concentrations), due to different number of moles of cations within the ionic diodes. The table shows that for ions with the same charge concentration, cations with higher valence have lower coefficients. These results also validated our experimental results from EIS: diodes with high-valence cations exhibited low diffusion coefficients.

Based on the Fick's first law[46] (see details in the supplementary information), we can further investigate the diffusion flux. As the charge concentration remained to be the same for our diodes with different cations, a lower diffusion coefficient results in a lower diffusion flux. Consequently, this reduction curtailed backward currents through the PN interface under the backward electric field, ultimately enhancing the rectification effects.
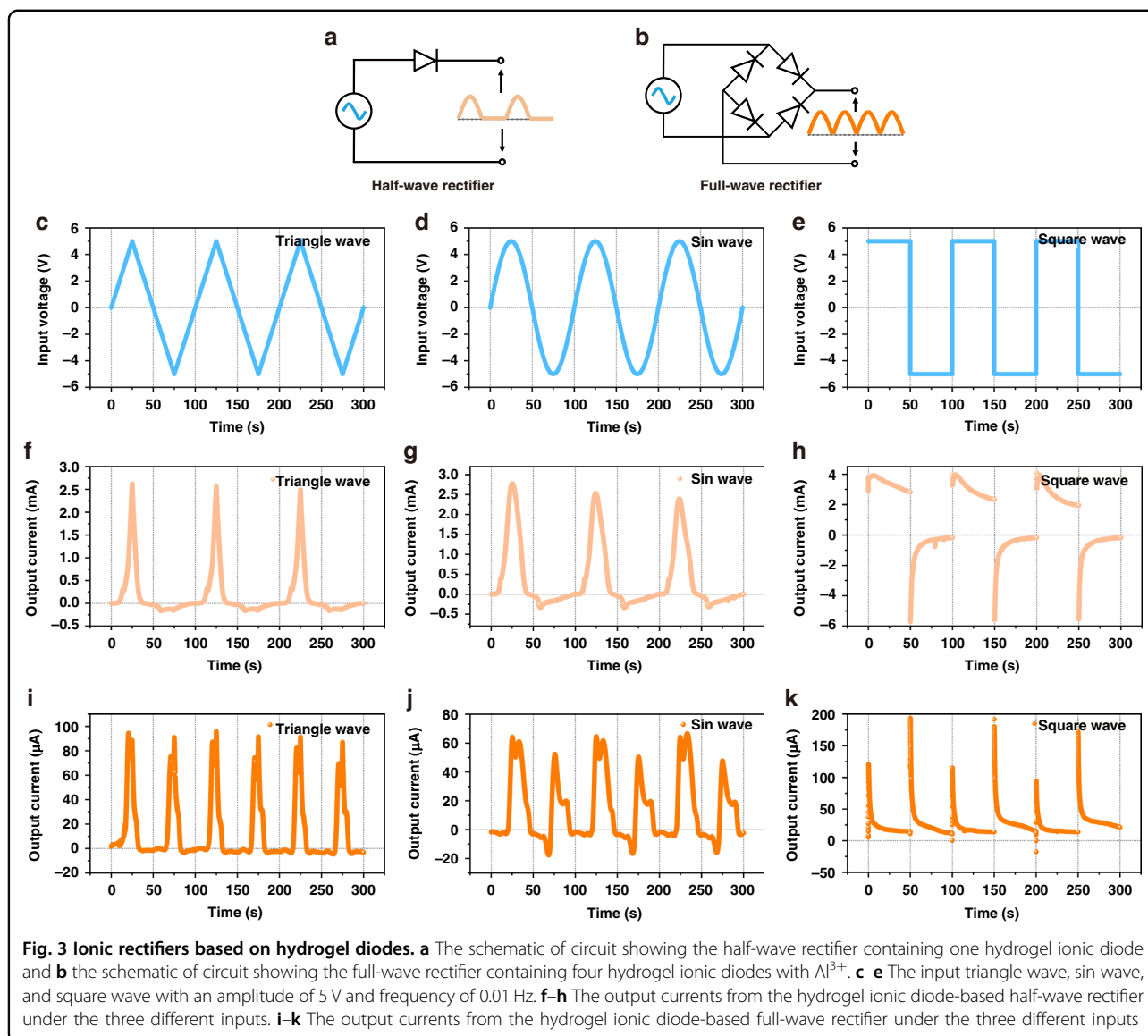
Most biological tissues, such as skin, exhibit stretchability ranging from 0% to 100%[47]. Considering the potential applications of ionic diodes in biological settings, we set 100% strain as our target stretchability. The modified hydrogel diode containing high-valence cations (e.g., Al^{3+}) can be stretched to more than 100% without breaking and maintain a good rectification ratio (>140) at 100% strain (Fig. 2h). Thanks to the interfacial adhesion at the PN junction, there is no layer separation and the hydrogel diodes can maintain the electrical functions during stretching. The increased rectification ratio with the strain can be attributed to the reduction in thickness of the hydrogel diode, which promotes the efficiency of ion migrations. Both I–V curves at the strain of 0% and 100% show a clear asymmetric current response, exhibiting an "on" state under the forward electric field (e.g. 5 V) and an "off" state under the backward electric field (e.g. −5 V). The high stretchability of our hydrogel ionic diodes surpasses that of nano-membrane or nano-channel based fluidic diodes, and the enhanced rectification ratio by using high-valence cations exceeds that of most stretchable ionic diodes ever reported (Figs. 2i, S10, and Table S3). This is also the first work on enhancing the rectification effect of ionic diodes through tailoring the properties of charge carriers and improving the electrical performance at the material level. In comparison to other methods, such as adopting highly-porous or reactive electrodes, shrinking down the size of PN junctions, and adjusting the structure of ionic diodes, our approach offers greater versatility across various application scenarios and can be seamlessly integrated with previously proposed methods. For instance, by shrinking down the size of PN junctions we can further increase the rectification ratio, as demonstrated by our stretched ionic diodes that exhibited thinner thickness and higher rectification ratio.

Soft iontronics based on optimized hydrogel diodes

The improved rectification effect of our hydrogel diodes allows us to apply them in iontronics. Here, we selected hydrogel diode with Al^{3+} due to its elevated rectification ratio. We first demonstrated ionic half-wave rectifier and full-wave rectifier by integrating the hydrogel diodes into circuits (Fig. 3a, b). By applying the input waves with an amplitude of 5 V and frequency of 0.01 Hz (Fig. 3c–e), the half-wave rectifier constructed with a single diode can successfully pass half of the input waves (including triangle wave, sin wave, and square wave) and block the other (Fig. 3f–h). The full-wave rectifier integrated by four diodes converted the input into output with the same polarity (Fig. 3i–k). We also applied input waves with a higher frequency of 0.05 Hz, the outputs from the half-wave rectifier shows larger reverse leakage currents that were not fully blocked, but the results still show a satisfactory ability to rectify input electric signals (Fig. S11). The presence of larger reverse leakage currents can be attributed to the limitation of ion mobility in response to higher frequencies, indicating the importance of selecting an appropriate frequency range when employing ionic diodes in iontronics.

Additionally, we fabricated a soft negative–positive–negative bipolar junction transistor (NPN BJT) based on two N-type hydrogel layers with trivalent cations Al^{3+} attached to one P-type hydrogel layer with monovalent anions Cl^- (Fig. 4a). We first validated the functioning of the two PN junctions by setting the collector voltage (V_C) to 0 V and applying a square wave with an amplitude of 5 V and a frequency of 0.05 Hz at the base as the input: base voltage (V_B) (Fig. 4a). When V_B was 5 V and V_C was 0 V, the base became positively polarized, causing the two PN junctions to be at the "on" state, thereby allowing the base current (I_B) to flow from the base to the collector and emitter. Thus, positive I_B and positive collector current (I_C) were obtained (Fig. 4b), with I_C being lower than I_B due to current division from I_B. On the contrary, when V_B was −5 V and V_C was 0 V, the base became negatively polarized, and the two PN junctions were at the "off" state. As a result, no currents could flow through the two PN junctions, and both I_C and I_B remained close to 0 (Fig. 4b). These results suggested that the two PN junctions were functioning correctly, and the BJT would conduct only when the base was positively polarized. Then, we applied a base current I_B (ranging from 0 to 0.6 mA) at the base and measured the collector current I_C in response to the collector voltage V_C. When V_C was negative, the base-collector junction was at the "off" state, allowing only limited currents (e.g., induced by ion diffusion) to pass this junction, thereby keeping I_C low. It should be noted that when I_B was 0 mA, the BJT was in the cut-off region and could not be operated. However, when $I_B > 0$ mA and $V_C > 0$ V, the base-collector junction was at the "on" state, allowing the BJT to operate. With the increase of V_C (from 0 to 1.5 V), the BJT started to conduct. Under a fixed V_C, I_C increased with the input I_B, showing a clear saturation region, where both the base-collector and base-emitter junctions were forward-biased (Fig. 4c). As V_C continued to increase, the emitter voltage (V_E) would equal the base voltage V_B, causing the base-emitter junction to become reverse-biased, allowing few currents to pass the base-emitter junction. As a consequence, all the
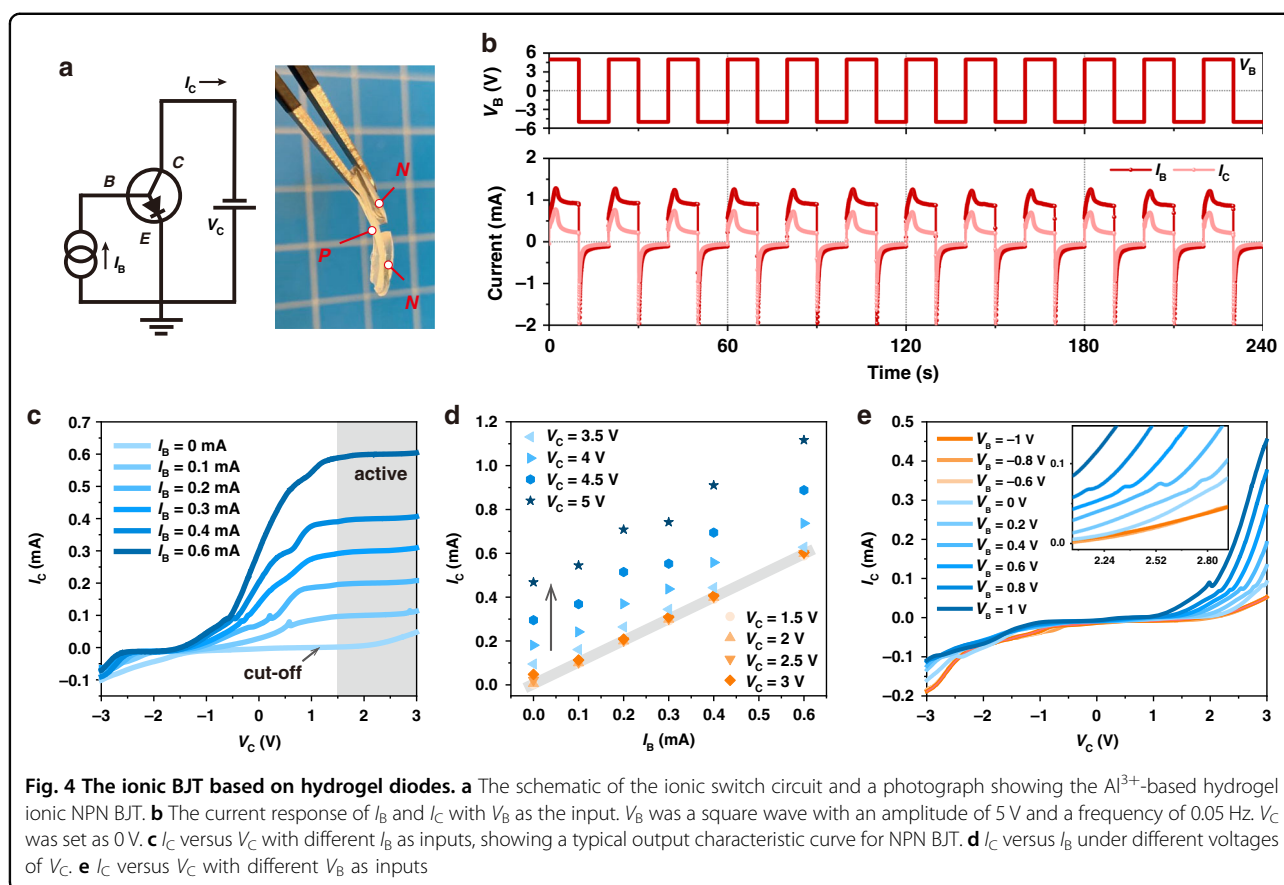
Fig. 3 Ionic rectifiers based on hydrogel diodes. a The schematic of circuit showing the half-wave rectifier containing one hydrogel ionic diode and **b** the schematic of circuit showing the full-wave rectifier containing four hydrogel ionic diodes with Al^{3+}. **c**–**e** The input triangle wave, sin wave, and square wave with an amplitude of 5 V and frequency of 0.01 Hz. **f**–**h** The output currents from the hydrogel ionic diode-based half-wave rectifier under the three different inputs. **i**–**k** The output currents from the hydrogel ionic diode-based full-wave rectifier under the three different inputs

current from the base I_B flowed to the collector, and I_C remained constant regardless of V_C (from 1.5 to 3 V), making the BJT reach the active region. However, as V_C continued to increase (from 3 to 5 V), I_C increased accordingly with I_B (Fig. 4d). This was because V_C was high enough to make the base-emitter junction "breakdown" and currents flowed from the emitter to the base, and ultimately to the collector. Thus, this breakdown region led to enhanced ion injection at the emitter-base junction and made I_C increase with V_C accordingly (Fig. 4d). On the other hand, we have also applied a voltage input V_B at the base rather than applying the current input I_B. One can see that in the operating region where $V_C > 0$ V, I_C increased with the input V_B. This was because higher V_B enhanced the forward-bias for the two PN junctions in the BJT,

thereby increasing the current flow from the base to collector. All these results demonstrated that an ionic BJT can be successfully realized using our hydrogel ionic diodes. These demonstrations showcase the potential of our optimized hydrogel diodes for broader applications and more practical uses, such as soft semiconductor devices.

Discussion

To enhance the relatively low rectification ratio of the gel-based stretchable ionic diodes, we have modified the rectification effect by incorporating cations with high valence in the P-type hydrogel layer. Through neutralization reactions based on the monomer acid AAc (H^+) and added bases with different cations, we replaced the original monovalent H^+ with high-valence cations

Fig. 4 The ionic BJT based on hydrogel diodes. a The schematic of the ionic switch circuit and a photograph showing the Al^{3+}-based hydrogel ionic NPN BJT. **b** The current response of I_B and I_C with V_B as the input. V_B was a square wave with an amplitude of 5 V and a frequency of 0.05 Hz. V_C was set as 0 V. **c** I_C versus V_C with different I_B as inputs, showing a typical output characteristic curve for NPN BJT. **d** I_C versus I_B under different voltages of V_C. **e** I_C versus V_C with different V_B as inputs

such as divalent cations Mg^{2+} and Ca^{2+}, and trivalent cations Al^{3+} and In^{3+}. It was found that the rectification effect of hydrogel ionic diodes can increase with the valence of incorporated cations. The trivalent cations (e.g., In^{3+}) enabled an enhanced rectification ratio of >70, significantly higher than that (rectification ratio: ~3) using monovalent cations. This enhancement was due to the higher valence of cations leading to a lower ion diffusion, which reduced the diffusion flux of cations and backward currents through the PN interface under the backward electric field, and ultimately enhanced the rectification effects. Moreover, our hydrogel ionic diodes can be stretched to over 100% strain and possess an increased rectification ratio of >140. The high stretchability of our hydrogel ionic diodes surpasses that of conventional nano-membrane or nano-channel based fluidic diodes, and the enhanced rectification ratio achieved by employing high-valence cations exceeds that of most stretchable ionic diodes reported to date. This work is also the first attempt to enhance the rectification effect of ionic diodes through the tailored properties of charge carriers (e.g., cations) and the improvement of electrical performance at the material level. The enhanced rectification effect enabled improved electrical performance and allowed us to apply the hydrogel diodes in iontronics such as rectifiers and BJT. We demonstrated the functionality of a half-wave rectifier, full-wave rectifier, and NPN BJT using the modified ionic diode, highlighting its potential in developing integrated ionic circuits or bioinspired iontronics based entirely on ions as charge carriers. While we only modified the valence of cations in the P-type layer, it is conceivable that tuning the valence of anions in the N-type layer or altering the structure of polyelectrolytes (e.g., highly branched polyelectrolytes) could also impact the rectification effect. Additionally, employing methods to incorporate mobile ions with higher valence, such as direct chemical synthesis of polyelectrolytes with high-valence mobile ions, may further enhance the rectification effect. Compared to electrons, there is a wider variety of naturally occurring ions that could be utilized in iontronics. As the famous architect Zaha Hadid has ever raised and adhered to: "There are 360 degrees. Why stick to one?", this principle can be applied to the construction of electronics based on ions. Drawing inspiration from biological systems that employ varying ions as charge carriers rather than the single electrons, the manipulation of different ion properties and the utilization of soft materials in iontronics could potentially unlock more versatile and expansive applications for future ion-based electronics.

Materials and methods

Materials

Acrylamide (AAm, A8887-2.5KG), agarose (Agar, A953 9-100G), crosslinker N, N'-methylenebis(acrylamide) (MB AA, 146072-100G), photoinitiator 2-hydroxy-4'-(2-hydro xyethoxy)-2-methylpropiophenone (Ir2959, 410896-50G), [2-(Acryloyloxy)ethyl]trimethylammonium chloride [DA C(Cl⁻), 496146-200ML], acrylic acid (AAc, 8.00181.05 00), sodium hydroxide (NaOH), potassium hydroxide (KOH), magnesium hydroxide [$Mg(OH)_2$], calcium hydroxide [$Ca(OH)_2$], aluminum hydroxide [$Al(OH)_3$], aluminum chloride ($AlCl_3$), and indium (III) chloride ($InCl_3$) were purchased from Sigma Aldrich.

Preparation of hydrogel ionic diodes

The P-type hydrogels and N-type hydrogels were first prepared separately, and then physically attached to form the hydrogel diode. The hydrogels were prepared by a one-pot method[36]. Briefly, for N-type hydrogels, 200 mg Agarose, 0.025 mol AAm, 0.0125 mol DAC(Cl^-), 0.0375 mol MBAA, 0.042 g Ir2959 (0.5 mol% of AAm), and 10 mL DI water were added into a beaker. The mixture was heated at 100 °C and stirred for 20 min until achieving a transparent solution. The precursor solution was then perfused into the 70 mm × 70 mm × 1 mm mold and cooled at 4 °C to form the first agarose network. Then, the cured hydrogel was photopolymerized under UV (365 nm, $10\,mW\,cm^{-2}$) for one hour to form the second copolymer network. The prepared double-network hydrogels were sealed in Ziploc bag and stored under 4 °C for further use. For P-type hydrogels with original H^+ as mobile cations, 200 mg Agarose, 0.025 mol AAm, 0.0125 mol AAc(H^+), 0.0375 mol MBAA, 0.042 g Ir2959 (0.5 mol% of AAm), and 5 mL DI water were added into a beaker. For P-type hydrogels with replaced cations M^{m+} as mobile cations, 100 mg agarose, 0.025 mol AAm, 0.0125 mol AAc(H^+), 0.0375 mol MBAA, 0.042 g Ir2959 (0.5 mol% of AAm), and 5 mL DI water were added into a beaker. The bases were added into the beaker with the amount of (0.0125/m) mol $M(OH)_m$ [e.g., 0.0125 mol NaOH, or 0.00625 mol $Mg(OH)_2$, or 0.0042 mol $Al(OH)_3$], to replace the original H^+ through neutralization reactions. The mixtures were then heated at 100 °C and stirred for 20 min until achieving a transparent solution. Curing the P-type hydrogels followed the same procedure with that for the N-type hydrogels. To prepare the hydrogel diodes, the cured P-type hydrogel piece and N-type hydrogel piece were physically stacked together. All the hydrogel diodes were sealed in Ziploc bags and stored at 4 °C before testing.

Electrical characterization

The current response of the hydrogel ionic diodes was measured using a source meter (Keithley 2602A, Keithley Instrument Inc.). The hydrogel ionic diodes have a diameter of 8 mm and thickness of 2 mm. Platinum wires were used as electrodes for the electrical measurement. Forward electric bias of 5 V and backward electric bias of −5 V were applied to the ionic diode to perform long-term (>80 s) current response of the ionic diodes. The forward current was the current response under 5 V and the backward current was measured under −5 V. The I–V curves of different ionic diodes were measured by the source meter through sweeping the voltage from 5 to −5 V. The AC-impedance spectra were measured by an electrochemical workstation (Metrohm Autolab), with testing frequency ranging from 10 MHz to 0.1 Hz. The input amplitude was 10 mV and a negative bias of −5 V was applied. To measure the rectification performance of the diodes under strain, the hydrogel ionic diodes were stretched to strains of 0%, 25%, 50%, 75%, and 100%, and the I–V responses were characterized under different strains.

Demonstrations of the iontronics

For the rectifiers, a function generator (33500B, KEY-SIGHT) was used to supply input, and the output was measured by a source meter. For the BJT, a DC power supply (UC305, UNIROI) was used to provide V_B, and the source meter was used to provide I_B. The source meter was used to record the I–V responses.

Author contributions
P.X. and X.L. designed the experiments, prepared the figures, and wrote the manuscript. P.X. prepared the materials, performed the mechanical and electrical characterizations, and conducted the demonstrations. X.W. conducted data analysis and provided assistance in preparing the figures. Z.Z. provided assistance on the material preparation and characterizations. P.P. provided assistance on the data analysis and experimental design.

Conflict of interest
The authors declare no competing interests.

References
1. Koo, H. J. & Velev, O. D. Ionic current devices—recent progress in the merging of electronic, microfluidic, and biomimetic structures. *Biomicrofluidics* **7**, 31501 (2013).
2. Siwy, Z. S. & Howorka, S. Engineered voltage-responsive nanopores. *Chem. Soc. Rev.* **39**, 1115–1132 (2010).

3. Schwab, A. Function and spatial distribution of ion channels and transporters in cell migration. *Am. J. Physiol. Ren. Physiol.* **280**, F739–F747 (2001).

4. Johansson, R. S. & Flanagan, J. R. Coding and use of tactile signals from the fingertips in object manipulation tasks. *Nat. Rev. Neurosci.* **10**, 345–359 (2009).

5. Abraira, V. E. & Ginty, D. D. The sensory neurons of touch. *Neuron* **79**, 618–639 (2013).

6. Daiguji, H., Oka, Y. & Shirono, K. Nanofluidic diode and bipolar transistor. *Nano Lett.* **5**, 2274–2280 (2005).

7. Cayre, O. J., Suk, T. C. & Velev, O. D. Polyelectrolyte diode: Nonlinear current response of a junction between aqueous ionic gels. *J. Am. Chem. Soc.* **129**, 10801–10806 (2007).

8. Han, J. H., Kim, K. B., Kim, H. C. & Chung, T. D. Ionic circuits based on poly electrolyte diodes on a microchip. *Angew. Chem. Int. Ed.* **48**, 3830–3833 (2009).

9. Koo, H. J., Chang, S. T. & Velev, O. D. Ion-current diode with aqueous gel/sio2 nanofilm interfaces. *Small* **6**, 1393–1397 (2010).

10. Tybrandt, K., Larsson, K. C., Richter-Dahlfors, A. & Berggren, M. Ion bipolar junction transistors. *Proc. Natl Acad. Sci. USA* **107**, 9929–9932 (2010).

11. Kim, Y. et al. A bioinspired flexible organic artificial afferent nerve. *Science (80-.)* **360**, 998–1003 (2018).

12. Sun, J. Y., Keplinger, C., Whitesides, G. M. & Suo, Z. Ionic skin. *Adv. Mater.* **26**, 7608–7614 (2014).

13. Yuk, H., Zhang, T., Parada, G. A., Liu, X. & Zhao, X. Skin-inspired hydrogel-elastomer hybrids with robust interfaces and functional microstructures. *Nat. Commun.* **7**, 1–11 (2016).

14. Kim, H. J., Chen, B., Suo, Z. & Hayward, R. C. Ionoelastomer junctions between polymer networ of fixed anions and cations. *Science (80-.)* **367**, 773–776 (2020).

15. Boutry, C. M. et al. A hierarchically patterned, bioinspired e-skin able to detect the direction of applied pressure for robotics. *Sci. Robot.* **3**, 1–10 (2018).

16. Kim, J. et al. Stretchable silicon nanoribbon electronics for skin prosthesis. *Nat. Commun.* **5**, 5747 (2014).

17. Yao, G. et al. Bioinspired triboelectric nanogenerators as self-powered electronic skin for robotic tactile sensing. *Adv. Funct. Mater.* **30**, 1–9 (2020).

18. Lopes, P. A., Paisana, H., De Almeida, A. T., Majidi, C. & Tavakoli, M. Hydroprinted electronics: ultrathin stretchable Ag–In–Ga E-skin for bioelectronics and human–machine interaction. *ACS Appl. Mater. Interfaces* **10**, 38760–38768 (2018).

19. Karnik, R., Duan, C., Castelino, K., Daiguji, H. & Majumdar, A. Rectification of ionic current in a nanofluidic diode. *Nano Lett.* **7**, 547–551 (2007).

20. Gracheva, M. E., Vidal, J. & Leburton, J. P. P-n semiconductor membrane for electrically tunable ion current rectification and filtering. *Nano Lett.* **7**, 1717–1722 (2007).

21. Ali, M., Ramirez, P., Mafé, S., Neumann, R. & Ensinger, W. A pH-tunable nanofluidic diode with a broad range of rectifying properties. *ACS Nano* **3**, 603–608 (2009).

22. Peng, R. et al. Ionotronics based on horizontally aligned carbon nanotubes. *Adv. Funct. Mater.* https://doi.org/10.1002/adfm.202003177 (2020).

23. Ying, B., Wu, Q., Li, J. & Liu, X. An ambient-stable and stretchable ionic skin with multimodal sensation. *Mater. Horiz.* **7**, 477–488 (2020).

24. Wang, L. et al. A metal-electrode-free, fully integrated, soft triboelectric sensor array for self-powered tactile sensing. *Microsyst. Nanoeng.* **6**, 59 (2020).

25. Yi, F. et al. Self-powered trajectory, velocity, and acceleration tracking of a moving object/body using a triboelectric sensor. *Adv. Funct. Mater.* **24**, 7488–7494 (2014).

26. Han, S. H. et al. Hydrogel-based iontronics on a polydimethylsiloxane microchip. *ACS Appl Mater. Interfaces* **13**, 6606–6614 (2021).

27. Kim, H. J., Chen, B., Suo, Z. & Hayward, R. C. Ionoelastomer junctions between polymer networks of fixed anions and cations. *Science (80-.)* **776**, 773–776 (2020).

28. Kumar, S. et al. Ultra-stretchable yet tough, healable, and biodegradable triboelectric devices with microstructured and ionically crosslinked biogel. *Nano Energy* **100**, 107438 (2022).

29. Mathwig, K., Aaronson, B. D. B. & Marken, F. Ionic transport in microhole fluidic diodes based on asymmetric ionomer film deposits. *ChemElectroChem.* **5**, 897–901 (2018).

30. Rong, Y. et al. Electrochemistry communications pH-induced reversal of ionic diode polarity in 300 nm thin membranes based on a polymer of intrinsic microporosity. *Electrochem. Commun.* **69**, 41–45 (2016).

31. Choi, E., Wang, C., Chang, G. T. & Park, J. High current ionic diode using homogeneously charged asymmetric nanochannel network membrane. *Nano Lett.* **16**, 2189–2197 (2016).

32. Huang, X., Kong, X. Y., Wen, L. & Jiang, L. Bioinspired ionic diodes: from unipolar to bipolar. *Adv. Funct. Mater.* https://doi.org/10.1002/adfm.201801079 (2018).

33. Nakayama, A. et al. High mechanical strength double-network hydrogel with bacterial cellulose. *Adv. Funct. Mater.* https://doi.org/10.1002/adfm.200305197 (2004).

34. Haque, M. A., Kurokawa, T. & Gong, J. P. Super tough double network hydrogels and their application as biomaterials. *Polymer* https://doi.org/10.1016/j.polymer.2012.03.013 (2012).

35. Liu, X., Liu, J., Lin, S. & Zhao, X. Hydrogel machines. *Mater. Today* https://doi.org/10.1016/j.mattod.2019.12.026 (2020).

36. Chen, Q., Zhu, L., Zhao, C., Wang, Q. & Zheng, J. A robust, one-pot synthesis of highly mechanical and recoverable double network hydrogels using thermoreversible sol–gel polysaccharide. *Adv. Mater.* **25**, 4171–4176 (2013).

37. Nyamayaro, K. et al. The rectification mechanism in polyelectrolyte gel diodes. *Phys. Fluids* **33**, 032010 (2021).

38. Fosbøl, P. L., Stenby, E. H. & Thomsen, K. Diffusion in multicomponent mixed solvent electrolyte systems. *Fluid Phase Equilib.* **584**, 114126 (2024).

39. Nyamayaro, K. et al. Toward biodegradable electronics: ionic diodes based on a cellulose nanocrystal-agarose hydrogel. *ACS Appl. Mater. Interfaces* **12**, 52182–52191 (2020).

40. Macounová, K., Electrochem, J., Soc, A., Wang, C. & Sastry, A. M. Electrochemical behavior of nanocrystalline electrodes in double-layer region. https://doi.org/10.1149/1.2783774 (2007).

41. Jiang, F. et al. Ion rectification based on gel polymer electrolyte ionic diode. *Nat. Commun.* **13**, 6669 (2022).

42. Lockett, V. N., Energy, P., Sedev, R. & Ralston, J. Differential capacitance of the electrical double layer in imidazolium-based ionic liquids: influence of potential, cation size, and temperature article differential capacitance of the electrical double layer in imidazolium-based ionic liquids: Influence of potential, cation size, and temperature. *J. Phys. Chem. C* **112**, https://doi.org/10.1021/jp7100732 (2008).

43. Lockett, V., Horne, M. & Sedev, R. Differential capacitance of the double layer at the electrode/ionic liquids interface. *Phys. Chem. Chem. Phys.* **12**, 12499–12512 (2010).

44. Dimaculangan, D. A. A. Determination of diffusion coefficients of heavy metal ions (Ni^{3+}, Zn^{2+}, Ba^{2+}, and Mn^{2+}) at infinite dilution through electrolytic conductivity measurements. *ASEAN J. Chem. Eng.* **22**, 58–71 (2022).

45. Kadhim, M. J. & Gamaj, M. I. Estimation of the diffusion coefficient and hydrodynamic radius (Stokes radius) for inorganic ions in solution depending on molar conductivity as electro-analytical technique—a review. *J. Chem. Rev.* **2**, 182–188 (2020).

46. Sulaiman, D. N. H. P., Suhaimi, H. & Shamsuddin, N. Estimating glucose diffusion coefficient of membranes for tissue engineering applications using Fick's First Law. *IOP Conf. Ser. Mater. Sci. Eng.* **991**, 0–7 (2020).

47. Vatankhah-Varnosfaderani, M. et al. Mimicking biological stress–strain behaviour with synthetic elastomers. *Nature* **549**, 497–501 (2017).